Lidar monitoring of water vapor and comparison with numerical simulations

F. De Tomasi(^{1}), P. Martano(^{2}), M. Miglietta(^{2}), A. Morabito(^{2})
and M. R. Perrone(^{1})

(^{1}) *INFM, Dipartimento di Fisica - Via per Arnesano, 73100 Lecce, Italy*
(^{2}) *Istituto per lo Studio dell'Inquinamento Atmosferico e l'Agrometeorologia*
    s.p. Lecce-Monteroni, 73100 Lecce, Italy

Summary. — A solar blind Raman (SBR) lidar based on a KrF excimer laser (248 nm) has been used to continuously monitor the water vapour mixing ratio in the lower troposphere and it is shown once more that the SBR lidar is a valuable tool for day- and night-time studies of the fine structure often seen in water vapour profiles. The lidar measurements of water vapour have been used to assess the performance of atmospheric boundary layer oriented mesoscale simulations. The Regional Atmospheric Modelling System (RAMS) has been used in this paper, to simulate circulation patterns and the planetary boundary layer structure over the Sallentum peninsula of Italy. Numerical simulations with different grid nesting, initialisation conditions and surface information details have been tested, and a satisfactory accordance between experimental and numerical water vapour profiles has been observed. It is shown that the sensitivity of water vapour profiles to the mixing height and surface advection effects can be successfully used for a proper testing of models especially in coastal areas and non-homogeneous terrain.

PACS `92.70.Cp` – Atmosphere.
PACS `92.60.-e` – Meteorology.
PACS `92.60.Fm` – Boundary layer structure and processes.

1. – Introduction

Water vapour is one of the most important state variables of the atmosphere because of its role in understanding several atmospheric processes such as radiative transfer, cloud formation, and energy transport. Then, a continuous monitoring of water vapour is of peculiar importance for meteorological, climatological and environmental studies [1]. Passive radiometers, satellite observations and active methods based on pulsed lasers are currently used for measuring atmospheric water vapour. Passive radiometers have poor vertical resolution, and are unable to observe the distinctive structure often seen in water vapour profiles [2]. Observations from satellite provide broad geographic coverage

but are limited both in accuracy and altitude resolution. The Raman lidar and the DIAL (Differential Absorption Lidar) techniques are instead well established for measuring water vapour with good range resolution and continuously. The DIAL systems exploiting the differential absorption of water vapour at two different laser wavelengths near 724 nm, have the potential to yield water vapour profiles with high vertical and temporal resolution as well as with an absolute error lower than 5% in the whole troposphere [3]. However, these active systems are rather complicated and require a high level of stability for the laser wavelengths as a consequence of the small bandwidth at the water absorption line [4]. Raman lidar systems make use of only one laser wavelength. The early work of Melfi *et al.* in the late 1960's [1] developed the technique of Raman spectroscopy in the measurement of tropospheric water vapour and since then several teams have contributed to the development of Raman lidars, especially for water vapour profiling [5]. Note that daytime measurements of water vapour are of peculiar interest: many important meteorological phenomena such as convective storm development occur more often during daytime than at night and so solar blind Raman (SBR) lidars working during both day and night have been developed [6]. Lidar systems based either on KrF (248 nm) excimer lasers [7] and on Nd:YAG lasers [8] operating in a frequency-quadrupled mode (266 nm) have been developed for daytime measurements of water-vapour, being the optimum operation wavelength located between 260 and 265 nm [6].

Tropospheric water vapour measurements performed at the University of Lecce (40° 20′ N, 18°6′ E) by a SBR lidar based on a KrF laser (248 nm) are reported in this paper, and the potentiality of continuous water vapour measurements to validate atmospheric models is exploited. The Regional Atmospheric Modelling System (RAMS), a mesoscale atmospheric model developed by Pielke *et al.* [9], has been used in this paper to simulate circulation patterns and the planetary boundary layer (PBL) structure over the Sallentum peninsula of Italy. The RAMS model is widely used for its completeness and flexibility that in turn imply a high degree of sensitivity in tuning the parameters during the simulations. Mesoscale models generally require a proper tuning, since effects that are usually negligible at the synoptic scale (*e.g.*, rotational) or at the microscale (*e.g.*, non-hydrostatic), can become important in the mesoscale simulations. The comparison of simulations with experimental data is then of fundamental importance to validate the tuning, in order to get quantitative reliable results from numerical models.

Two RAMS simulations with different grid nesting, initialisation conditions and surface information details have been tested in this paper to investigate the performance of atmospheric boundary layer oriented mesoscale simulations: the first with a very local initialisation and the second using information from regional scale analysis fields. The methodology and the lidar set-up are firstly described in the paper, then the water-vapour measurements conducted in Lecce on July 27th-28th, 1999 are presented (sect. **2**). The comparison of lidar data with the RAMS results is presented and discussed in sect. **3**.

2. – Lidar set-up and measurements

As is well known, the water vapour mixing ratio r can be measured as a function of range z by means of the Raman lidar signals of water vapour, nitrogen and oxygen [6]

$$(1) \qquad r(z) = K[S_{H_2O}(z)/S_{N_2}(z)] \, [S_{O_2}(z)/S_{N_2}(z)]^\gamma \,,$$

TABLE I. – *Spectroscopic Raman data for an incident wavelength of 248 nm.*

Species X	Raman shift (cm^{-1})	Scattered wavelength (nm)	Raman backscattering cross-section (m^2 sr^{-1})
O_2	1556	257.9	2.68×10^{-33}
N_2	2330	263.7	1.30×10^{-33}
H_2O	3653	273.2	4.10×10^{-33}

where K is a calibration factor; the factor with the oxygen Raman signal eliminates the effect of ozone absorption and

$$(2) \qquad \gamma = [\Delta\sigma(H_2O, N_2)] / [\Delta\sigma(N_2, O_2)] \,,$$

where $\Delta\sigma(X,Y)$ is the ozone absorption cross-section difference for the Raman wavelength λ_X and λ_Y. Equation (1) is obtained by assuming either that ozone is the only factor of wavelength-dependent attenuation [6], or that each Raman signal is given by

$$(3) \qquad S_X(z) = k_X(d\sigma/d\Omega)_X(1/z^2)q(\lambda_0, z)q(\lambda_X, z)N_X \,,$$

where $(d\sigma/d\Omega)_X$ is the Raman backscattering cross-section for the species X, k_X is an instrumental factor, $q(\lambda, z)$ is the atmospheric transmission between ranges 0 and z, N_X is the concentration of the species X, and λ_0 is the laser wavelength. The main spectroscopic Raman data for an incident wavelength of 248 nm taken from literature are reported on table I.

The experimental set-up of the lidar system that makes use of a KrF laser (Lambda Physik LPX 210 i) operating at a repetition rate of 80 Hz as radiation source, is shown in fig. 1. A Newtonian telescope, whose primary mirror has 30 cm diameter and 120 cm focal length, collects the backscattered radiation. A 1.2 mm field stop aperture (D) located on the telescope focus limits its field of view to approximately 1 mrad. A 50% beam splitter (BS) divides the collected radiation into two channels. A double-grating monochromator (Jobin-Yvon DH10 UV) characterised by an out-band rejection lower than 10^{-7} and a spectral resolution of 0.4 nm, when used with a 0.5×8 mm^2 central slit, is used in each Raman channel to spectrally resolve the backscattered radiation. No cross talk between nearby lines has been observed. Each Raman signal is detected in the photon-counting regime by a photosensor module (Hamamatsu H5783p-06) connected to a 300 MHz discriminator (Phillips Scientific Mod. 6908) and a multichannel scaler (EG& G MCS-Mod. 914 P). Neutral density filters (F) in front of the monochromator are only required for N_2 and O_2 Raman signal measurements to reduce count rates. The system is remotely controlled by a home-developed software. The lidar system has only two Raman channels and as a consequence O_2 and N_2 signals are firstly measured to evaluate the effect of the boundary-layer ozone absorption accordingly to eq. (1). Then, H_2O and N_2 signals are measured. The ozone absorption profile is assumed to not change throughout the daytime hours, when water vapour measurements are carried out [6]. Indeed, the ratio $S_{O2}(z)$ / $S_{N2}(z)$ has not been observed to vary significantly with the time during one day or during few days. These results may be due to the fact that these measurements have been taken in a rural area. So, the authors believe that the assumption of constant ozone profile throughout the day hours is not too crude when
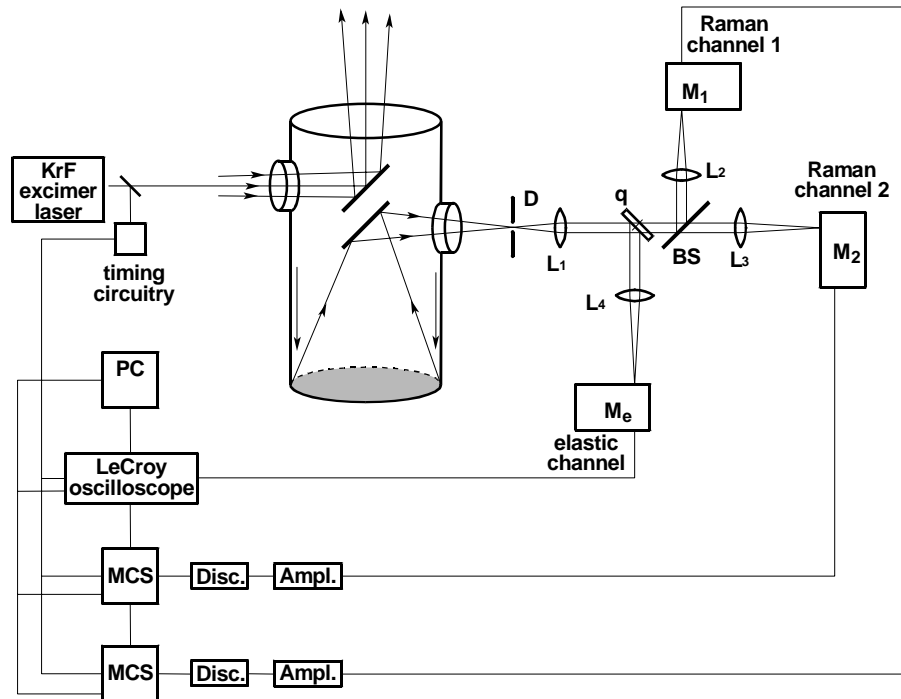
Fig. 1. – Schematic set-up of the lidar system; D, diaphragm; L, lenses; q, quartz plate; BS, beam splitter; M, monochromator and photosensor.

water vapour measurements are carried out in non populated areas, accordingly to [7]. Let us mention that at our wavelength extinction is mainly determined by ozone: in fact, the differential extinction due to Rayleigh scattering from atmosphere and Mie scattering from aerosols is negligible [6].

Figure 2 displays some water vapour profiles recorded at Lecce on July 27-28th, 1999 at different hours of the day. The water vapour profiles have been obtained by averaging 10^5 laser shots and the data have been smoothed with an average window length of 45 m. We have used *in* situ measurements taken at an altitude of 30 m to determine the calibration factor K in eq. (1). Indeed, the water vapour profile taken at 1300 (LST), which is characterised by a smooth variation in the lower layer, has been used to determine the K value by comparison with *in situ* measurements, in order to reduce errors due to the larger value of lidar minimum altitude. Note that the water vapour and nitrogen channel ratios have also been corrected for the range-dependent calibration ratios, due to differences between the two channels [10]. The profiles shown in fig. 2 represent the diurnal evolution of the water vapour mixing ratio in clear sky conditions. It is possible to observe from fig. 2 that the water vapour mixing ratio profiles get more homogeneous with altitude as the daytime activity increases, for the convective activity within the PBL that increases with the global solar radiation in clear sky conditions. A comparison of water vapour mixing ratio profiles measured by the lidar at Lecce and by a radiosounding balloon at Brindisi (40°39′ N, 15°57′ E) located near the Adriatic sea, about 35 km north-east wards of Lecce, are also shown on fig. 2 (dotted line) for sake of comparison. Sounding balloon measurements at the lidar site were not available.
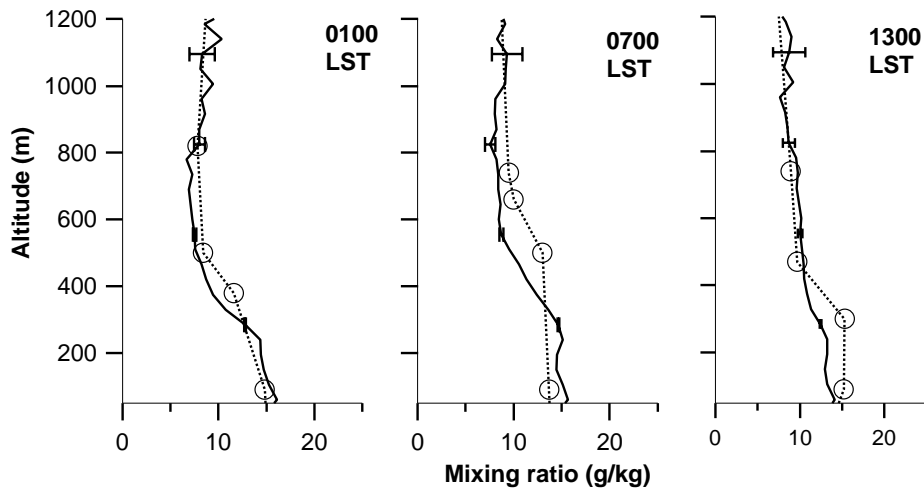
Fig. 2. – Water vapour mixing ratio profiles recorded at different day hours (LST) on July 28, 1999. Error bars indicate 1-σ uncertainty of the lidar measurements calculated by assuming Poisson statistics. The data have been smoothed with an average window length of 45 m. The dotted line shows the sounding balloon profile provided by the Italian Air Force located at Brindisi, about 35 km North-East from the lidar site.

In view of the spatial separation of the two experiments, there is a good accordance. This intercomparison gives confidence in the lidar calibration and measurements. It is believed that in flat regions, under stable meteorological conditions, and during nights with vanishing wind speed, advective motions are not expected to occur and the water vapour distribution is expected to be rather homogeneous within an area few ten of km wide. In fact, fig. 2 reveals a rather good accordance between lidar and sounding balloon measurements mainly at 0100 (LST).

The correlation between water vapour profiles and convective activity within the PBL is more clearly revealed by fig. 3 that shows the contour maps of the water vapour mixing ratio monitored continuously with the lidar system over a 28-hours period on July 27-28, 1999. Both days were characterised by clear sky conditions. It is remarkable, on July 27th, that the water vapour mixing ratio reaches values of about 12 g/kg at least up to 800 m during the daytime hours whereas at night, it reaches the value of 12 g/kg at about 250 m. As has been mentioned, this evolution is consistent with that of the PBL [11] that shows a great variability over land, strongly correlated to the insolation and to the orography of the area of interest [12]. The contour maps of the water vapour mixing ratio (fig. 3) also show that the PBL rises up to diurnal heights on the next day (July 28th). $r(z)$ reaches the value of 12 g/kg at least up to 400 m during the first daytime hours. However, it is worth observing that the altitudes where $r(z)$ reaches the value of 12 g/kg reduce faster after midday on this last day (July 28th): a possible interpretation of this last experimental result is given below and in sect. **3**.

Figure 4 display the time evolution during July 28th of ground measurements of temperature $T(°C)$, relative humidity $U(\%)$, water vapour mixing ratio $r(g/kg)$, and wind module $WM(m/s)$ provided by the local meteorological station. The incoming wind direction data are shown on fig. 5 (solid line). A first phase (0100 LST-0500 LST) characterised by typical stable night-time conditions with vanishing wind speed, decreasing
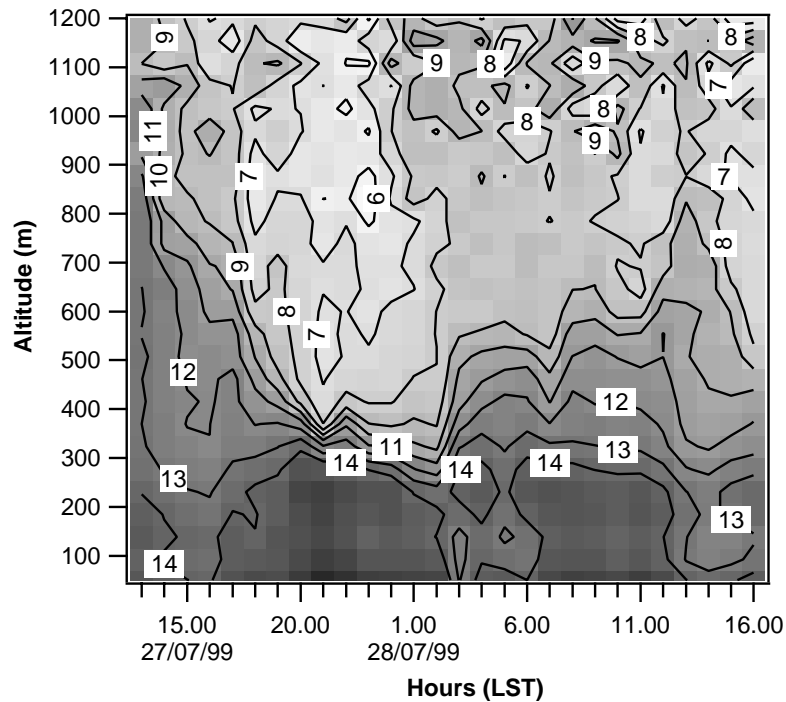
Fig. 3. – Contour maps of the water vapour mixing ratio (g/kg) of July 27-28, 1999.

of temperature and increasing of relative humidity near condensation is evident from fig. 4 on July 28th. A second phase occurs between 0600 and 0900 LST, during which the relative humidity decreases whereas the water vapour mixing ratio increases as a consequence of evaporation. Finally, a third phase is apparent after 0900 LST, where a definite increasing in speed and turning of the wind from the North (fig. 5) is associated to an increase of water vapour mixing ratio and temperature, that suggests marine air advection. It is worth observing that the marine air advection can be responsible of the fast increase of the water vapour mixing ratio observed on July 28th after midday, at the lower altitudes (fig. 3).

3. – The RAMS model: comparison of numerical and lidar data

The RAMS model developed at the Colorado State University [9] is a mesoscale atmospheric model with a quite detailed modulus on soil/vegetation parameterisation and boundary layer turbulence closure, with options between the first order [13] and the one-and-half order [14] schemes. The model works in terrain-following coordinates and has options between hydrostatic or non-hydrostatic modes and various top/lateral boundary conditions. Nested grids can be used to enhance resolution in areas of interest.

The RAMS model has been used in this paper to simulate the circulation patterns and the boundary layer structure over the Sallentum peninsula on July 28th, 1999: a clear sky day with high-pressure conditions over southern Italy. The geographic location, time of the year, and the choice of a cloudless day are ideal for evaluating models against observations: the large-scale atmosphere is almost undisturbed and forcing is primarily
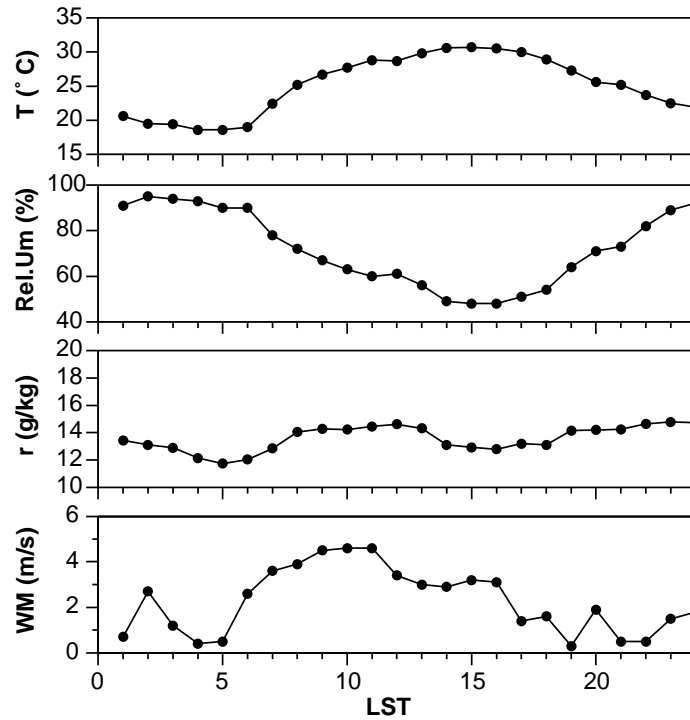
Fig. 4. – Meteorological data of July 28, 1999 measured by the station located at the lidar site at ~ 30 m from ground.
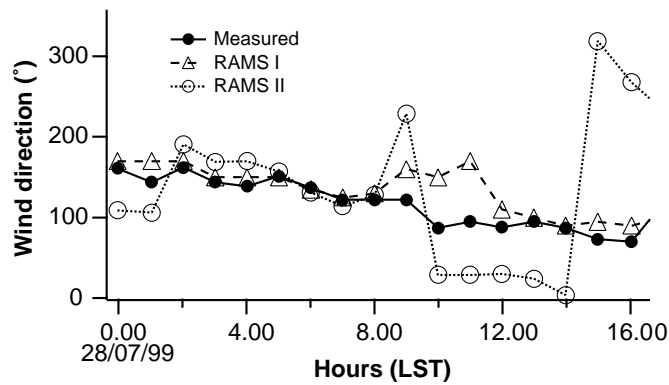
Fig. 5. – Incoming wind direction ground measurements at the lidar site (solid line). The dashed and dotted lines show the corresponding numerical profiles obtained with the first and the second RAMS simulation, respectively. The direction is in degrees counterclockwise with respect to the W-E axis.
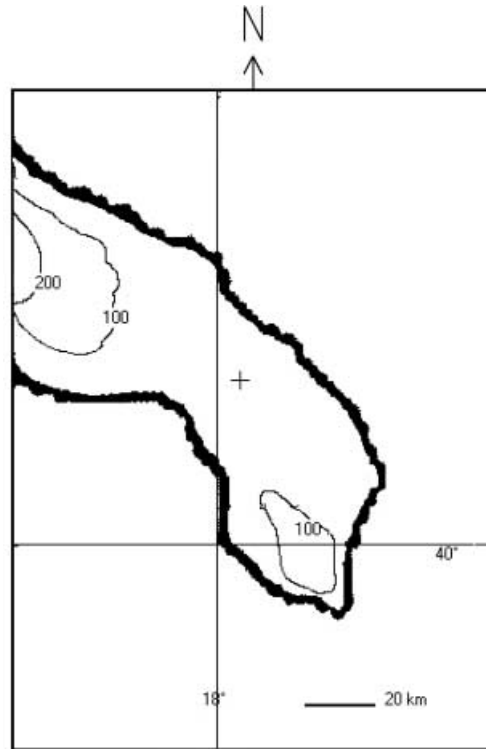
Fig. 6. – Map of the Sallentum region corresponding to the inner grid in the simulation. The cross indicates the measurements site.

local and surface based.

Two different RAMS simulations are presented here: the first is initialised with very local meteorological information, while the second "nudges" the outer boundaries of the domain with regional scale analysis fields.

The map of the region corresponding to the inner nested grid from which data are extracted, is shown in fig. 6. In the first RAMS simulation, two nested grids of 7.5 and 2.5 km step, respectively centred on the south Apulia and the Sallentum peninsula, have been used with 25 vertical levels. In particular, a vertical resolution of 100 meters in the lowest level, with a stretching factor of 1.2 up to 1000 meters in the upper levels, has been used. The domain height was at about 15 km. The version 3b of the model has been used hydrostatically with homogeneous initialisation through a single 0100 LST radiosounding profile for day 28th of July provided by the meteorological station of the Italian Air Force at Brindisi. The total simulation time was of 24 hours, since previous tests showed that the model tends to drift away in longer runs without a proper nudging on the boundaries. No significant spin off time is expected in this simulation, due to the homogeneous initialisation and the lack of a consistent orography in the site. The RAMS standard Sea Surface Temperature (SST) data file has been used for the monthly average of the SST distribution and a homogeneous soil/vegetation texture has also been used ("mixed woodland" landuse cathegory, for which the surface fluxes appeared to be in good agreement with some experimental data from sonic anemometers taken in
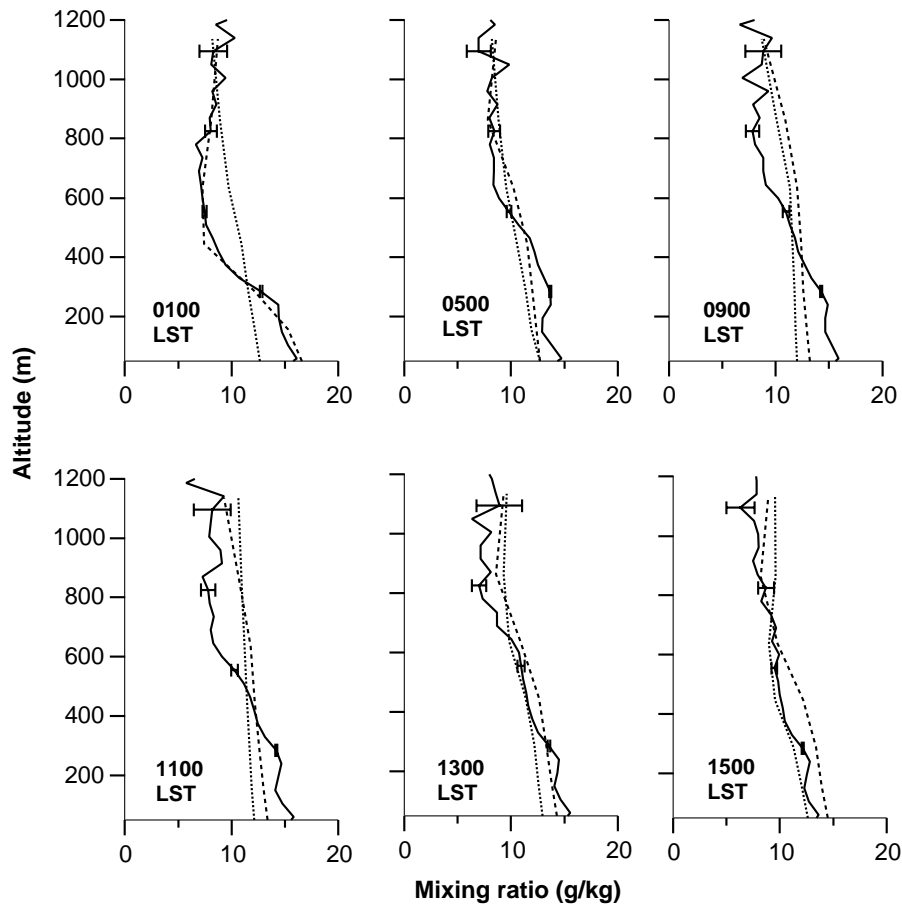
Fig. 7. – Water vapour mixing ratio lidar measurements (solid lines) and numerical profiles obtained by the first (dashed lines) and the second (dotted lines) RAMS simulation on July 28, 1999.

the dry season in the site). The soil surface initialisation has been set at $-2\,°C$ with respect to the surface air temperature at midnight, with a surface relative moisture of 0.1, characteristic of dry seasons in the site. Both the Smagorinsky and the Mellor-Yamada turbulence parameterisations have been tested and it has been found that the numerical results were not significantly affected. The results presented in the paper, referring to the first RAMS simulation, have been obtained by using the Smagorinsky turbulence parameterisation, since it allows an *ad hoc* tuning of the vertical diffusion coefficients.

Figure 7 shows the water vapour mixing ratio profiles provided by the first RAMS simulation (dashed lines) besides lidar profiles (solid lines). The accordance between experimental and numerical data that is good up to about 0500 LST worsens during the morning hours, since the numerical profiles tend to be more homogeneous. Indeed, a faster growth rate of the water vapour mixing ratio is observed in the profiles provided by the RAMS between 0700-1100 LST. The fast rise of PBL height that is revealed by the RAMS potential temperature profiles may be responsible of such differences (fig. 8a). In fact, the temperature profile at 1200 LST is typical of a well-established convective

situation. It is also worth noting from fig. 7 that RAMS (dashed lines) and lidar moisture profiles (solid line) get in closer accordance after midday. This may be due to the formation of a Thermal Internal Boundary Layer (TIBL) coming from a local turning of the wind from the northern direction. The time evolution of the wind direction at ground and at the lidar site provided by the RAMS simulation is shown on fig. 5 (dashed line). A wind turning from the Adriatic coast between 1100 and 1200 LST is revealed by fig. 5 (dashed line). It is believed that the wind turning favours the advection of cooler marine air, causing the formation of the TIBL at about 450 m, as it is revealed by the potential temperature profile at 1300 LST (fig. 8a). The wind turning is observed earlier, at about 0900 (LST), by the ground meteorological sensor at the lidar site (fig. 5, solid line). The delay in wind turning may be responsible of the differences between the water vapour mixing ratio profiles retrieved by the lidar measurements at 0900 and 1100 LST (fig. 7, solid lines) and the corresponding profiles provided by the RAMS simulation (fig. 7, dashed lines). The wind turning delay can be due to the lack of a proper time-depending boundary conditions for the model domain and to the rather poor representation of the sea surface temperature, initialised as local monthly average in the input data.

A second RAMS simulation with different grid nesting, initialisation conditions and surface information details has then been performed in order to better investigate the dependence of the correlation between numerical and experimental results on simulation constraints. A three-nested-grid system (36, 12 and 4 km step) respectively, with the vertical structure as in the previous simulation, but with nudging on the boundary of the largest one, has been used in the second RAMS simulation. The 6-hours-step meteorological fields provided by the European Center for Medium-range Weather Forecasts (ECMWF) have also been used. The 9 km resolution satellite SST data obtained from the daily NOAA AVHRR Oceans Pathfinder Sea Surface Temperature Data Set have been used for the SST. A more detailed non-uniform vegetation map adapted from the Corine Land Use Map, and local vegetation cover information [15], have been used for the two nested grids with the same soil humidity and temperature initialization as in the previous simulation. The ECMWF meteorological fields at 0100 (LST) of July 28th, 1999 and the sounding balloon measurements taken at the meteorological station of Brindisi at the same time, have been used for the model initialization. The ISAN data assimilation package of RAMS has been used for the first grid. Finally, the non-hydrostatic mode and the Mellor-Yamada turbulence closure scheme have been used in this last simulation. The total simulation time was again of 24 hours, and the apparent spin off time of the model wind field was of about 5 hours, and therefore it is believed that the boundary layer evolution and the wind field are not affected during the day.

The water vapor mixing ratio profiles provided by the second RAMS simulation are shown in fig. 7 (dotted lines). It is apparent from fig. 7 that the water vapor mixing ratio profile provided by the model at 0100 (LST) is quite different from the measured one. This is a consequence of the initialization conditions that make use of local data and ECMWF fields. However, the differences between numerical and lidar profiles reduce with time and get lower than 15% at 1300 hours (LST). Figure 7 (dotted lines) also shows that the numerical water vapor mixing ratio profiles provided by the second RAMS simulation are more homogeneous than the experimental ones (fig. 7, solid lines) during the morning hours, and this result lead to consider that a faster PBL growth occurs even in the second simulation. It is also worth observing from fig. 7 that the spatial and temporal evolution of the water vapor mixing ratio, obtained with the second simulation (dotted lines), get quite close to that obtained with the first simulation (dashed lines) after few hours from the starting simulation time. In fact, the differences between the
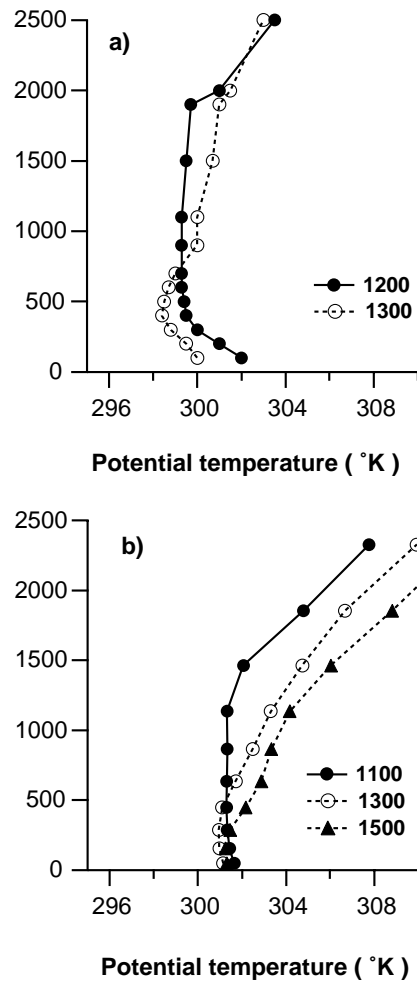
Fig. 8. – Potential temperature profiles at different hours of the day obtained by a) the first and b) the second RAMS simulation.

two numerical profiles are lower than 3% at 0500 (LST). Finally, fig. 7 shows that the numerical profiles get in closer accordance with the experimental ones after midday even in the second RAMS simulation. The marine air advection coming from wind turning seems, also in the second simulation, to be responsible of the closer accordance between experimental and numerical water vapor mixing ratio profiles, after midday. Figure 5 (dotted line) shows the temporal evolution of the wind direction provided by the second RAMS simulation and reveals that a wind turning from the coast (N-NE) occurs at about 1000 LST. The temporal evolution of the wind direction provided by the second RAMS simulation is during late morning, better correlated with the measured profile (fig. 5, solid line). In fact, the wind turning is revealed at about 0900 LST by the ground meteorological sensor at the lidar site. The better accordance in late morning, between the experimental and numerical evolution of the wind direction, is probably due to the better definition in the second RAMS simulation, of the SST and of the boundary

meteorological conditions. The potential temperature profiles obtained with the second RAMS simulation at 1100, 1300 and 1500 hours (LST) are shown in fig. 8b. The changes on the potential temperature profiles are around midday smaller than those observed at the lower altitudes, in the profiles provided by the first RAMS simulation (fig. 8a). The different turbulence closure that has been used in the two simulations can be responsible of this last result. However, the formation of a lower height TIBL is also revealed by the vertical evolution of the potential temperature profiles provided by the second simulation after 1300 LST (fig. 8b), may be due to the advection of stable marine air.

In conclusion, the time evolution of the water vapor mixing ratio profiles provided by the second RAMS simulation is similar to the one obtained with the first RAMS simulation, even if different grid nesting, initialization conditions, surface characteristics, and SST data have been used. The water vapor numerical profiles are more homogeneous than the measured ones during the morning hours, as a consequence of the faster growth rate of the PBL height, and the differences between numerical and experimental data reduce after midday. The numerical results provided by the second simulations lead also to consider that advection processes prevent the PBL to further develop in the early afternoon of July 28th, and as a consequence, a better accordance between experimental and numerical profiles is observed after midday. As has been mentioned, the contour maps of the water vapour mixing ratio of fig. 3 lead also to consider that the PBL height reduces faster after midday on July 28th.

4. – Conclusion

Measurements of tropospheric water vapour mixing ratio conducted with a solar blind Raman lidar at Lecce (40°20′ N, 18°6′ E) on July 1999 have been presented. The lidar profiles have been used to assess the performance of atmospheric boundary layer oriented mesoscale simulations. In fact, the moisture lidar profiles have been compared with those obtained by two different RAMS simulations. Different grid nesting, initialisation conditions, surface information details, and SST data have been used in the two RAMS simulations, and a satisfactory accordance between experimental and numerical water vapour profiles has been found. It has also been observed that the use of a three-nested-grid system, of local and ECMWF meteorological fields, of satellite SST data, and of more detailed land-use maps has not allowed significant improving of the accordance between numerical and experimental water vapour profiles. The water vapor numerical profiles provided by both simulations are more homogeneous than the measured ones during the morning hours, as a consequence of the faster rise of the PBL height. However, the differences between numerical and experimental profiles reduce after midday, in both simulations, since it is believed that advection effects prevent the PBL to further develop in the early afternoon of July 28th. Therefore, it has been shown that the sensitivity of the water vapour profiles to the mixing height and surface advection effects can be successfully used for a proper tuning of the boundary conditions of mesoscale meteorological models mainly in coastal areas and non-homogeneous terrain. We believe that the results presented in this paper show that the continuous lidar monitoring of water vapour can be of great interest in a detailed assessing of the performance of atmospheric boundary layer-oriented mesoscale simulations.

* * *

REFERENCES

[1] MELFI S. H. and WHITEMAN D., *Bull. Am. Meteorol. Soc.*, **66** (1985) 1288.
[2] VAUGHAN G., WAREING D. P., THOMAS L. and MITEV V., *Q. J. R. Meteorol. Soc.*, **144** (1988) 1471.
[3] WULFMEYER V., *Appl. Opt.*, **37** (1998) 3804.
[4] KIM D., CHA H., PARK J., LEE J. and VESELOVSKII I., *J. Korean Phys. Soc.*, **30** (1997) 458.
[5] KWON S. A., IWASAKA Y., SHIBATA T. and SAKAI T., *Atmosph. Environ.*, **31** (1997) 1459.
[6] RENAUT D. and CAPITINI R., *J. Atmosph. Oceanic Techn.*, **5** (1988) 585.
[7] EICHINGER W. E., COOPER D. I., ARCHULETTA F. L., HOF D., HOLTKAMP D. B., KARL R. R. JR, QUICK C. R. and TIEE J., *Appl. Opt.*, **33** (1994) 3923.
[8] WHITEMAN D. N., MELFI S. H. and FERRARE R. A., *Appl. Opt.*, **31** (1992) 3068.
[9] PIELKE R. A., COTTON W. R., WALKO R. L., TREMBACK C. J., NICHOLLS M. E., MORAN M. D., WESLEY D. A., LEE T. J. and COPELAND J. H., *Meteorol. Atmos. Phys.*, **49** (1992) 69.
[10] GOLDSMITH J. E. M., BLAIR F. H., BISSON S. E. and TURNER D. D., *Appl. Opt.*, **37** (1998) 4979.
[11] BELLECCI C., DALU G. A., AVERSA P., CASELLA L., FEDERICO S. and P. GAUDIO P., *SPIE*, **3865** (1999) 108.
[12] SANTACESARIA V., MARENCO F., BALIS D., PAPAYANNIS A. and ZEREFOS C., *Nuovo Cimento C*, **21** (1998) 585.
[13] SMAGORINSKY J., *Mon. Weather Rev.*, **91** (1963) 99.
[14] MELLOR G. L., YAMADA T., *Rev. Geophys. Space Phys.*, **20** (1982) 851.
[15] MARCHIORI S., Department of Biology, University of Lecce, Italy, private communications (1999).